

Morphology, crystallography and defects of the intermetallic χ -phase precipitated in a duplex ($\delta + \gamma$) stainless steel

A. REDJAMIA*

Laboratoire de Science et Génie des Surfaces, UMR-CNRS 7570, Ecole Européenne d'Ingénieurs en Génie des Matériaux et Ecole des Mines, Parc de Saurupt, 54042 Nancy Cedex, France

E-mail: redjamia@mines.inpl-nancy.fr

A. PROULT

Laboratoire de Métallurgie Physique, Université de Poitiers, UMR-CNRS 6630, bât SP2MI, Boulevards Pierre et Marie Curie, BP 30 179, F-86962 Futuroscope Cedex, France

P. DONNADIEU

L.T.P.C.M. INPG-ENSEEG, UMR-CNRS 5614, 1130 rue de la piscine, BP75 Domaine universitaire F-38402 Saint Martin D'Herès Cedex, France

J. P. MORNIROLI

Laboratoire de Métallurgie Physique et Génie des Matériaux, UMR-CNRS 8517, Université des Sciences et Technologies de Lille et Ecole Nationale Supérieure de Chimie de Lille, Cité Scientifique, 59655 Villeneuve d'Ascq Cedex, France

The ferritic matrix in the Fe-22Cr-5Ni-3Mo-0.03C ferritic-austenitic duplex stainless steel undergoes a variety of decomposition processes when aged in the temperature range 650–750°C. These processes involve the precipitation of the austenite and of the σ and χ Frank-Kasper phases. The intermetallic χ -phase is found at both the grains boundaries (homo and heterophase interfaces) and inside the ferritic grains where it adopts an unexpected hexagonal shape. At the early stage of its precipitation, it nucleates at the δ/γ and δ/σ heterophase interfaces and then grows by expanding exclusively in the ferritic matrix. This study is basically focused on this intermetallic χ -phase. The crystal structure and the chemical composition are respectively studied by electron diffraction and energy dispersive X-ray spectroscopy. The χ -phase exhibits rational orientation relationships with the austenite and the σ -phase with which it is in contact and an invariably cube-on-cube orientation relationship with the ferritic matrix into which it grows. Based on the orientation relationship, the morphology and the number of variants of this χ -phase are understood in terms of the group theory. The planar defects present in a large density in the χ -phase, are roughly parallel to $\{0\ 1\ 1\}_\chi // \{0\ 1\ 1\}_\delta$. The fault vectors are determined as: $\frac{1}{3}\langle 110 \rangle_\chi$ and $\frac{1}{4}\langle 111 \rangle_\chi$, the latter corresponding for a bcc structure to a π phase shift, the defects can be simply described as π boundaries. Based on the obtained results, a structural proximity between the χ -phase and a super-cell derived from the ferritic matrix has been brought to light. This super-cell is described as a stacking of corrugated and planar layers obeying the following parallelism $\{0\ 1\ 1\}_\chi // \{0\ 1\ 1\}_\delta$. Indeed this super-cell approach provides an interpretation for several microstructural features such as the χ/δ interface plane, the planar defects in the χ -phase and their related fault vectors.

It has been also stated that Mo is an efficient χ -phase forming element. Upon these considerations a detailed characterization provided valuable insights into the precipitation mechanism associated with the χ -phase formation.

© 2004 Kluwer Academic Publishers

* Author to whom all correspondence should be addressed.

1. Introduction

Duplex stainless steels are being increasingly used as structural materials in oil, chemical and power industries [1–4]. This is related to the fact that their duplex microstructure ($\delta + \gamma$) allows a beneficial mixture of austenitic (γ) and ferritic (δ) properties: on the one hand a high strength with a desirable toughness [5, 6] and, on the other hand, a good corrosion resistance, especially to chloride-induced stress corrosion cracking [7–9]. The Z3CND-22-05 with the nominal composition Fe-22Cr-5Ni-3Mo-0.03C (wt%) is a member of this family. This grade is now largely used as a standard material in offshore conditions [10]. The heat treatment of this duplex stainless steel leads to a series of metallurgical transformations, which take place in the ferrite or at its grain boundaries, apart from the martensite, which forms in the austenite [11, 12]. In a previous study [13], efforts were made to characterize the different products of the δ -ferritic matrix decomposition in the temperature range 400–1050°C. The characterization of the phase precipitation was best undertaken from the isothermal heat treatment of the fully δ -ferrite microstructure retained by water quenching to room temperature. This isothermal treatment induces the decomposition of the supersaturated δ -ferrite and produces various phases: the $M_{23}C_6$ and M_7C_3 carbides [11], the austenite (γ) with different shapes [11–14], the α' -BCC ferrite [11, 15, 16], the intermetallic G-phase [17], the novel τ -phase described elsewhere [18] and some undesirable secondary phases; the latter being mainly the sigma (σ) [11], R [19, 20] and khi (χ) [20] Frank-Kasper phases.

The intermetallic χ -phase, whose characterization is reported in the present paper belongs to the tetrahedrally close-packed (TCP) phases. The presence of this phase has been reported, for the first time, by Andrews and Brookes [21] in a steel containing Cr, Ni and Mo. McMullin *et al.* [22] have also established the existence of this intermetallic compound as an equilibrium phase, on isothermal sections of Fe-Cr-Mo ternary diagram in the temperature range 815–900°C. Kasper [23] analysed this phase in the alloy synthesized by McMullin *et al.* [22] and deduced that its chemical composition is $Fe_{36}Cr_{12}Mo_{10}$ and that its unit cell contains 58 atoms.

The crystal structure has been investigated by means of X-ray and neutron diffraction from powdered specimens. It was found that the χ -phase is an intermetallic compound whose structure is isomorphous with the well-known α -manganese [24]. This α -Mn structure is a departure from the Frank and Kasper rules [25]. According to these rules, the local close packed atomic arrangements should be consistent only with the coordination numbers 12, 14, 15 and 16; the coordination number 13 being forbidden. The most amazing features of the α -Mn structure is that the Mn atoms can occupy atomic sites having different coordination number meaning that Mn atoms have different sizes. It is found that the χ -phase structure can be considered as an ordered α -Mn structure where the Mo atoms occupy the largest atomic sites and the Cr atoms tend to segregate in the largest remaining sites (Table I). As a result, the χ -phase belongs to the space group $I\bar{4}3m$. Its cubic

TABLE I Position of atoms in the cell of the $Fe_{36}Cr_{12}Mo_{10}$ χ -phase [23]

Number of atoms (Wyckoff notation)	Coordination CN	x	y	z
2(a)	16	0	0	0
8(c)	16	0.317	–	–
24(g)	13	0.356	–	0.042
24(g)	12	0.089	–	0.278

unit cell with lattice parameter $a_\chi = 0.892$ nm contains 58 atoms, 24 of them having a 13 coordination number (Table I) [23].

The χ -phase is found in several binary systems involving transition metals. It frequently occurs in steels, as a ternary compound containing Fe, Cr and Mo, according to the composition $Fe_{36}Cr_{12}Mo_{10}$ [23]. This composition can vary in a large domain depending on the involved metallic atoms [26]. Okafor *et al.* [27] and Ritter *et al.* [28] have shown that the χ -phase obeys the following formula $Fe_{36}Cr_{12}Mo_3Ti_7$ and $Fe_{50}Cr_{33}Mo_{13}Ni_5$ in the quaternary Fe-Cr-Mo-Ti and Fe-Cr-Mo-Ni systems, respectively. The χ -phase can also be regarded as a carbon-dissolved compound that behaves either as an intermetallic compound or as a $M_{18}C$ type carbide [29].

The precipitation of the χ -phase is accelerated by cold working [30, 31] while its amount is increased by the nitrogen content [32]. The nucleation sites are the grain boundaries, the incoherent twin boundaries and the intragranular dislocations [30]. Occasionally, it also nucleates at coherent twin boundaries [30]. Frequently, the χ -phase grows from $M_{23}C_6$ carbides, which dissolve after ageing at high temperatures [33]. In stainless steel, it is usually associated with the σ Frank-Kasper phase [20].

It is well established that the precipitation of the χ -phase leads to a reduction of the creep ductility due to a good resistance to brittle microcracking [34]. It has also a reverse effect on the toughness and corrosion properties [35]. A substantial depletion of solid solution strengtheners (like Cr, Mo, C and N) mainly due to a copious precipitation of the χ -phase beyond one hundred hours results in a strong decrease of the yield strength [36].

These mechanical properties have to be connected with the nucleation features, the microstructural distributions and the morphology as well as with their crystallographic orientations and lattice misfits.

Several investigations [34–39] have reported the χ -phase precipitation during isothermal heat treatments of steels. However, detailed characterization of the intermetallic χ -phase, in any kind of stainless steels and especially in duplex stainless steels is not available. Such a characterization is of extreme significance because it is expected to provide valuable insights into the precipitation mechanism associated with the χ -phase formation. Thus, the aim of this investigation is basically devoted to the study of the χ -phase precipitated within the ferritic δ -matrix of a duplex stainless steel as a consequence of isothermal heat treatment. TEM and electron diffraction are used to identify the crystal

structure and to characterize the crystal defects of the χ -phase. It is also intended, through this study, to explain the equilibrium shape of the χ -phase and its formation mechanism by using transmission electron microscopy (TEM) coupled with energy-dispersive X-ray spectroscopy (EDS). The derived information will be used as a basis for studying the structural similitude between the χ -phase and the ferritic δ -matrix where it takes place.

2. Material and experimental procedure

The as-received Fe-22Cr-5Ni-3Mo-0.03C (wt%) duplex austenitic-ferritic ($\delta + \gamma$) specimens were solution treated at 1375°C for 20 min in order to achieve homogeneity. They were subsequently water quenched to retain a supersaturated and fully ferritic (δ) microstructure. The specimens were then heat treated in the temperature range 650–970°C for various times (up to 336 h), followed by water-cooling. All the treatments were carried out in electric muffle furnaces under vacuum to minimize oxidation. The chemical composition of the supersaturated ferrite and of its decomposition products is listed in Table II.

Thin foils for electron microscopy were prepared following conventional TEM sample preparation methods. The samples were mechanically polished up to the lowest possible thickness (about 20 μm) and then electropolished at 40 V in a solution of 5% perchloric acid in 95% II-butoxyethanol with a Struers Tenupol twin-jet unit. They were investigated with two transmission electron microscopes: a Philips CM 12 microscope and a Jeol 200 CX microscope operated at 120 and 200 kV, respectively. A double-tilt cooling specimen holder was used. Diffraction patterns were obtained in the selected-area electron diffraction (SAED) mode with a parallel incident beam and also in the convergent beam electron diffraction (CBED) mode with a nearly parallel electron beam focussed on a very small area of the thin foil. High Resolution Electron Microscopy (HREM) was performed on a Philips EM 430 ST electron microscope operated at 300 kV. The optimum point-to-point resolution was better than 0.2 nm. This instrument is equipped with a Tracor-Northern analysis energy-dispersive X-ray spectroscopy (EDS) analysis system. The EDS spectrometer is interfaced with a minicomputer to log the spectra and to conduct qualitative or quantitative analyses. Quantitative analysis of EDS spectra without standards was performed assuming the thin film approximation, i.e.: no absorption. The Cliff-Lorimer expression for concentration ratios was used,

TABLE II Elemental partitioning of ferrite and intermetallic χ -phase. Comparison with the surrounding and unaged ferrite

Phase	Elements (wt%)					
	Fe	Mo	Cr	Mn	Ni	Si
δ_{unaged}	68.8	2.5	22.5	1.6	5.1	0.5
δ	70.3	0.9	22.4	2.5	2.9	0.7
χ	48.3	22.5	22.9	2.9	2.5	0.7

relying on k factor values calculated for K spectral lines.

An X-ray diffractometer, with a Co K_{α} radiation, was used to determine with accuracy the lattice parameter of the body-centred cubic (BCC) ferritic matrix. This lattice parameter is used as a calibration to measure the lattice parameter of the χ -phase.

3. Experimental results

3.1. Microstructural features

Isothermal heat treatments in the temperature range 650–750°C produce, in addition to the austenite and the intermetallic σ -phase, heavily faulted χ -phase particles. This phase, which always occurs after the σ -phase precipitation, is detected only by transmission electron microscopy (TEM). It is neither observed by optical microscopy nor detected by X-ray diffraction due to the small size and the limited amount of these precipitates.

The χ -phase particles are found both inside the ferritic grains and at the grain boundaries. TEM observations show that the χ -phase particles present inside the ferritic grains appear as hexagonal plates when projected along $\langle 111 \rangle_{\delta}$ directions (Fig. 1a). The directions of these χ/δ interfaces were determined by trace analysis involving a great number of δ -matrix orientations. It was established that these facets are parallel to $\{011\}_{\delta}$.

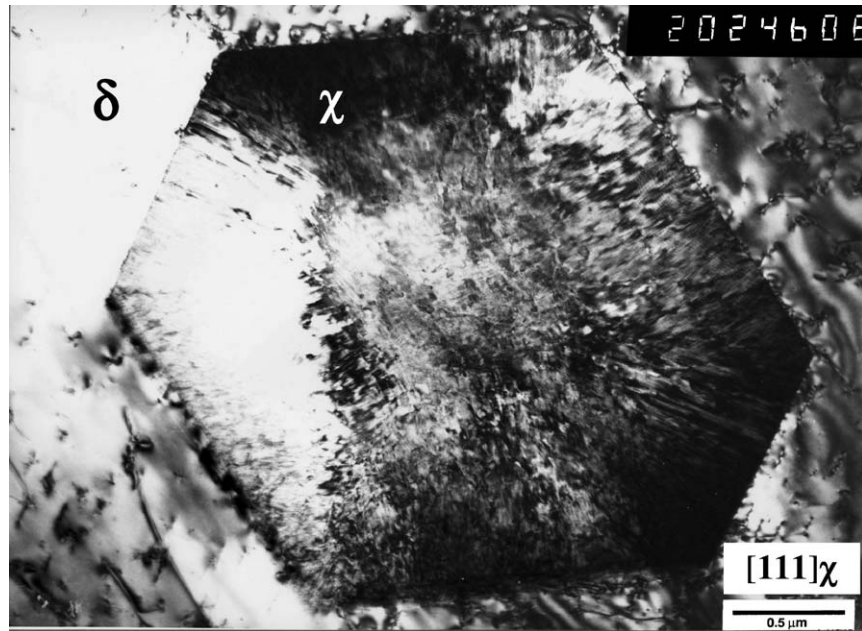
In the early stages of the χ -phase precipitation, some particles are also observed at both the δ/γ and δ/σ heterophase interfaces. The χ -phase particles developed at these heterophase interfaces expand exclusively in the δ -ferritic matrix (Fig. 1b and c). At δ/γ interfaces, they exhibit a semi-hexagonal shape (Fig. 1b). Particles nucleated at δ/σ interfaces develop unspecified shapes (Fig. 1c). Note that orientation relationships will be reported in Section 3.3 and related morphologies will be discussed in Section 4.2.

The χ -phase precipitation reaction displays a C-curve kinetic with its nose located around 700°C. The incubation time at this temperature is estimated to be around 200 h; it corresponds to the formation of χ -phase particles detectable from TEM observations [13]. At lower temperature, the χ -phase appears after the σ -phase precipitation. In fact, the precipitation domain of the χ -phase is included in that of the σ -phase [13].

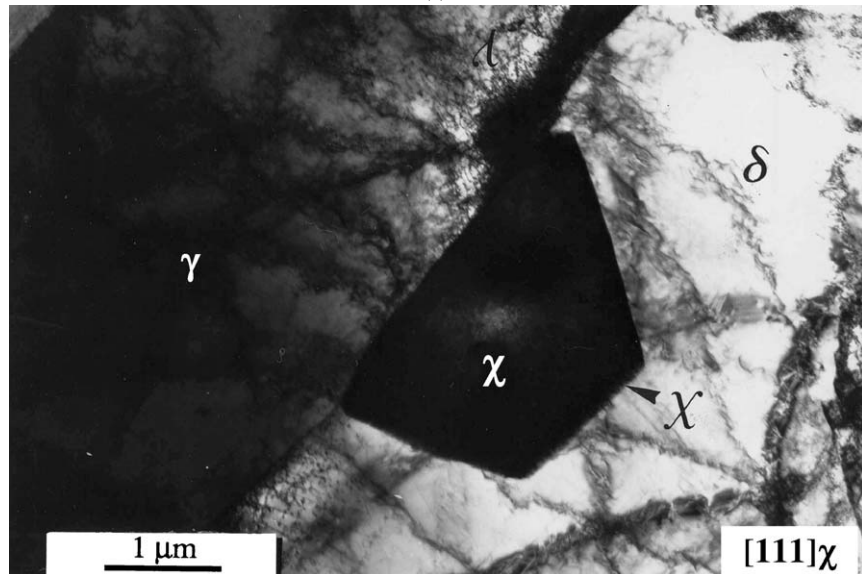
3.2. Electron diffraction identification of the χ -phase

In this section, we intend to identify the crystallographic features of the χ -phase from electron diffraction patterns.

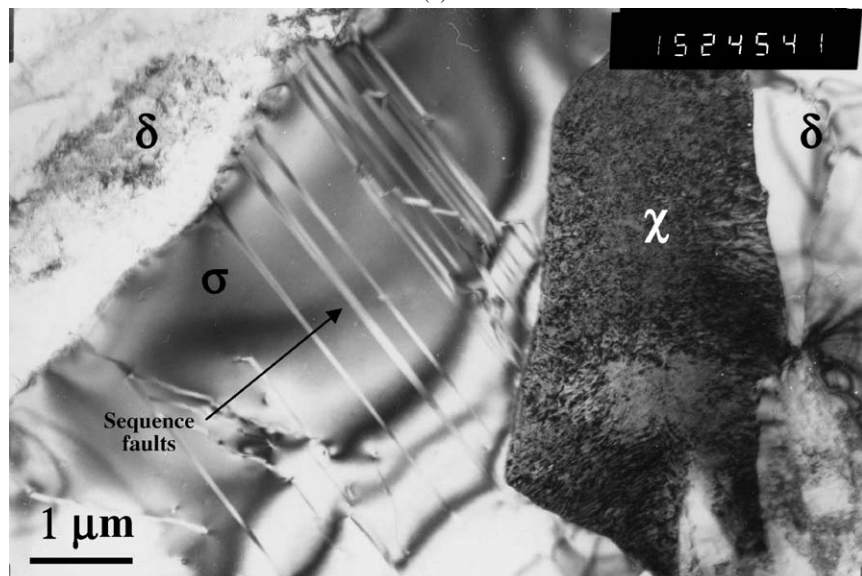
Two-dimensional (2D) and especially three-dimensional (3D) symmetry information required for the space group identification [40] is not available on the CBED patterns from the heavily faulted χ -phase particles. This is mainly due to the large lattice parameters of the χ -phase which strongly limit the possibility of beam convergence. As a result, the diameter of the transmitted and diffracted disks is very small and not enough details are visible inside these



(a)



(b)



(c)

Figure 1 (a) Bright field TEM image showing a hexagonal χ -phase particle embedded in the δ -ferritic matrix. (b) Bright field TEM image showing χ -phase particle developed at the interface δ/γ and expanded in the δ -ferritic matrix. (c) Bright field TEM image showing χ -phase particle developed at the interface δ/σ and expanded in the δ -ferritic matrix. The straight lines in the σ -phase are sequence faults.

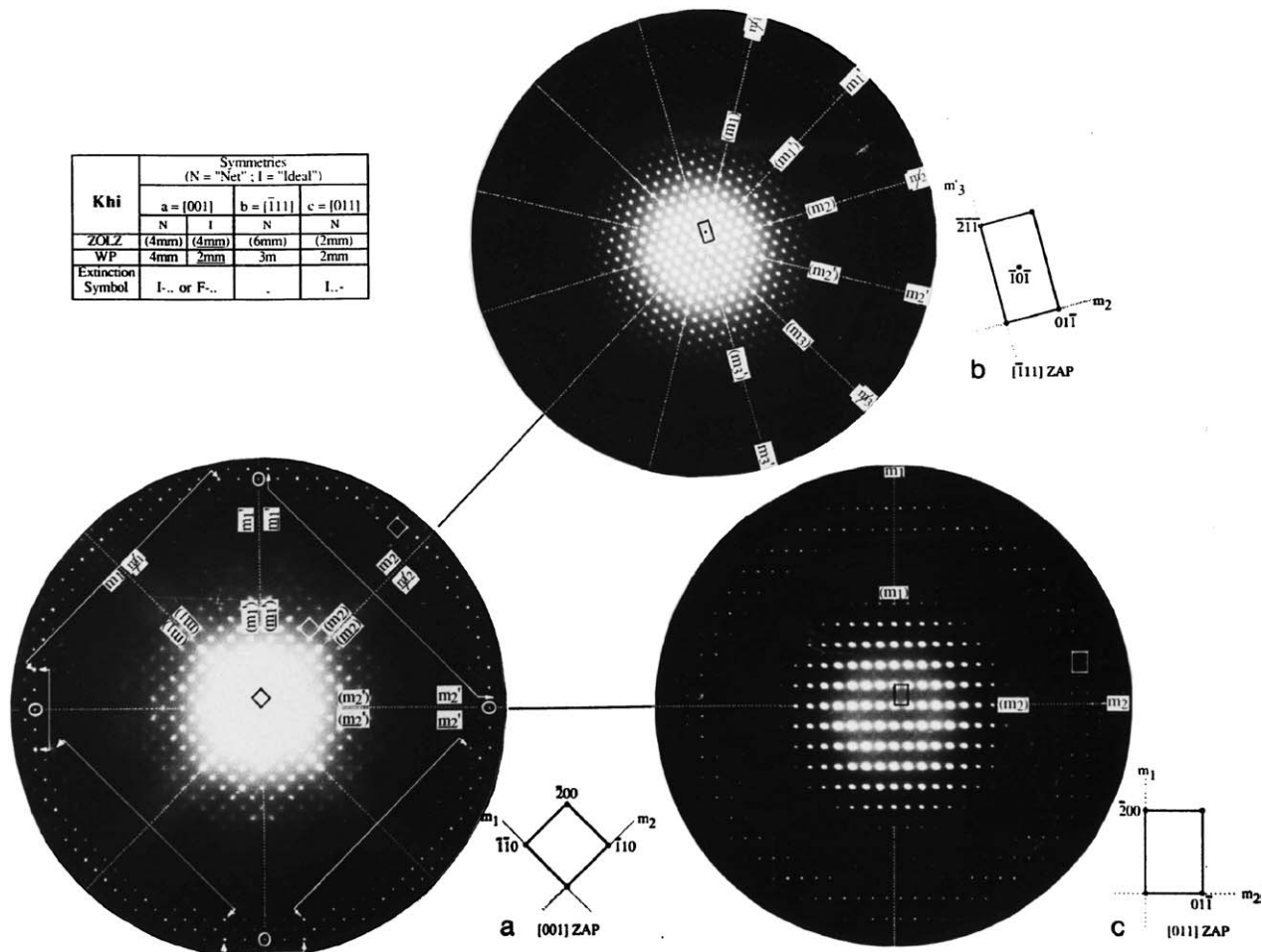


Figure 2 Whole pattern (ZOLZ + FOLZ symmetry information) for the cubic χ -phase: (a) [001] zone axis microdiffraction pattern, showing $\{(4mm), 4mm\}$ "net" and $\{(4mm), 2mm\}$ ideal symmetries. The absence of ZOLZ/FOLZ periodicity difference indicates that there is no glide plane perpendicular to the [001] direction and that the partial extinction symbol is $I\bullet\bullet$ or $F\bullet\bullet$. (b) $[-111]$ zone axis microdiffraction pattern showing $\{(6mm), 3m\}$ "net" symmetries. (c) [011] zone axis microdiffraction pattern showing $\{(2mm), 2mm\}$ "net" symmetries. The absence of ZOLZ/FOLZ periodicity difference indicates that there is no glide plane perpendicular to the [011] direction and that the partial extinction symbol is $I\bullet\bullet$.

disks to infer the pattern symmetries with confidence. Despite this difficulty, Morniroli and Steeds [41] have shown that many important crystal features can be obtained through zone axis patterns (ZAPs) performed by focusing a nearly parallel electron beam onto a very small specimen area. The microdiffraction patterns, thus obtained, are composed of small diameter disks grouped into Zero and High Order Laue Zones (ZOLZ and HOLZ). These patterns allow the identification of:

- The "net" and "ideal" symmetries¹ The "net" symmetry is concerned with the position of the reflections on the pattern while the "ideal" symmetry is concerned with both the position and the intensity of the reflections. These symmetries are in connection with the crystal system and with the point group, respectively.
- The shift between the ZOLZ and the FOLZ (First Order Laue Zone) reflection nets. It is related to the Bravais lattices.

- The periodicity difference between the ZOLZ and the FOLZ reflection nets. It is in connection with the presence of glide planes.

The crystal features of the χ -phase were determined from microdiffraction patterns according to a systematic method described elsewhere [41]. Among the investigated zone axis patterns, it appears that the highest "net" symmetries are observed for two ZAPs. The first one displays the symmetries (4mm), 4mm (Fig. 2a) and the second one the symmetries (6mm), 3m (Fig. 2b). According to Tables VII and II in [41], these symmetries correspond to a cubic system and to the $\langle 001 \rangle$ and $\langle 111 \rangle$ ZAPs. The specific ZAPs to investigate in order to identify the Bravais lattice and the possible glide planes are $\langle 001 \rangle$ (Fig. 2a) and $\langle 110 \rangle$ (Fig. 2c).

On the $\langle 001 \rangle$ ZAP, two sets of perpendicular "net" mirrors m_1, m_2 , and m'_1, m'_2 are identified (Fig. 2a). The smallest squares drawn in the ZOLZ and in the FOLZ reflections have their sides parallel to the m_1, m_2 mirrors and are identical. In addition, FOLZ reflections are present on the m'_1, m'_2 mirrors but absent on the m_1, m_2 mirrors. In agreement with Fig. 9d in [41], the corresponding partial extinction symbol is either $I - \bullet\bullet$ or $F - \bullet\bullet$ meaning that the distinction between the I and

¹The notation for the "net" and "ideal" symmetries of the ZOLZ and of the Whole Pattern (WP) and for the partial extinction symbols are given in accordance with those used in reference [41].

TABLE III Space and point groups for extinction symbol $I----$

Extinction symbol	Space groups	Point groups
$I----$	$I23$	23
	$I2_13$	
	$Im\bar{3}$	$m\bar{3}$
	$I432$	432
	$I4_132$	
	$I\bar{4}3m$	$\bar{4}3m$
	$I\frac{4}{m}\bar{3}\frac{2}{m}$	$\frac{4}{m}\bar{3}\frac{2}{m}$

F Bravais lattices is impossible from the observation of this unique $\langle 001 \rangle$ ZAP.

The $\langle 110 \rangle$ ZAP (Fig. 2c) exhibits $(2mm)$, $2mm$ “net” symmetries. No FOLZ reflections are present on the two perpendicular m_1 and m_2 mirrors and the two rectangles with their sides parallel to the mirrors are identical in the ZOLZ and in the FOLZ. Comparison with Fig. 9d in [41] leads to the partial extinction symbol $I - \bullet\bullet$.

Addition of these two partial extinction symbols gives $I----$. As indicated on Table 3.2 of the International Tables for Crystallography [42], this extinction symbol is in agreement with the seven space groups belonging to the five point groups given in Table III.

The point group must be identified in order to make the distinction between these seven possible space groups. This can be done from observations of the $\langle 001 \rangle$ ZAP “ideal” symmetry (see Table VIII in Ref. [41]). Actually, this $\langle 001 \rangle$ pattern (Fig. 2a) exhibits a $(4mm)$ “ideal” ZOLZ symmetry but a careful examination of the intensity of some pairs of reflections (see for example the pairs of reflections arrowed on Fig. 2a) reveals that the “ideal” symmetry of the whole pattern is only $2mm$ since the two “net” mirrors m_1 and m_2 are no longer “ideal” mirrors if the intensity of the reflections is taken into account. The corresponding point group is $\bar{4}3m$ and therefore the space group is $I\bar{4}3m$. These electron diffraction results are in agreement with those established by Kasper [23] using X-ray and neutron diffraction.

It is pointed out that a great care should be taken to identify the “ideal” symmetry since this symmetry takes into account the intensity of the reflections. The intensity (but not the position) of the reflections strongly depends on the crystal orientation and on the specimen thickness. To overcome this difficulty, the specimens were perfectly aligned with respect to the incident beam and a very small spot size (in the range 20–100 nm) was chosen in order to reduce the possible thickness and orientation variation in the diffracted area. Some experiments were also performed at low temperature. A low temperature increases strongly the intensity of the FOLZ reflections and therefore makes easier the identification of the “ideal” symmetry.

The lattice parameter $a_\delta = 0.2876 \text{ nm}$ of the δ -matrix, measured from X-ray diffraction patterns, is used to calibrate the electron diffraction patterns and then to deduce the lattice parameter of the χ -phase. In such a way we obtained $a_\chi = 0.894 \text{ nm}$. Note that this parameter is very close to three times that of the ferritic matrix. This result is also in good agreement with that given in the literature [23].

All the theoretical electron diffraction patterns were obtained with the Electron diffraction software [41].

3.3. Orientation relationships

It is obvious that χ -phase particles have definite orientation relationships with respect to the δ -matrix where they grow as well with the two other phases γ and σ whose interfaces γ/δ and σ/δ act as nucleation sites.

3.3.1. χ/δ relationship

Zone axis patterns (ZAPs) from the χ/δ interfaces (Fig. 3a) are composed of weak reflections belonging to the χ -phase and strong ones from the δ -matrix. Their analysis shows that both the inter and intragranular χ -phase particles adopt invariably a cube-on-cube orientation relationship with the ferritic matrix. As a result, there is a parallelism between planes and directions having the same indices, i.e.:

$$\begin{aligned} (0\ 0\ 1)_\chi & // (0\ 0\ 1)_\delta \\ (0\ 1\ 1)_\chi & // (0\ 1\ 1)_\delta \\ (1\ 1\ 1)_\chi & // (1\ 1\ 1)_\delta \end{aligned}$$

These relationships are in agreement with those first established by Thompson *et al.* [38] but they disagree with those reported by Zakine *et al.* [43].

3.3.2. χ/γ orientation relationship

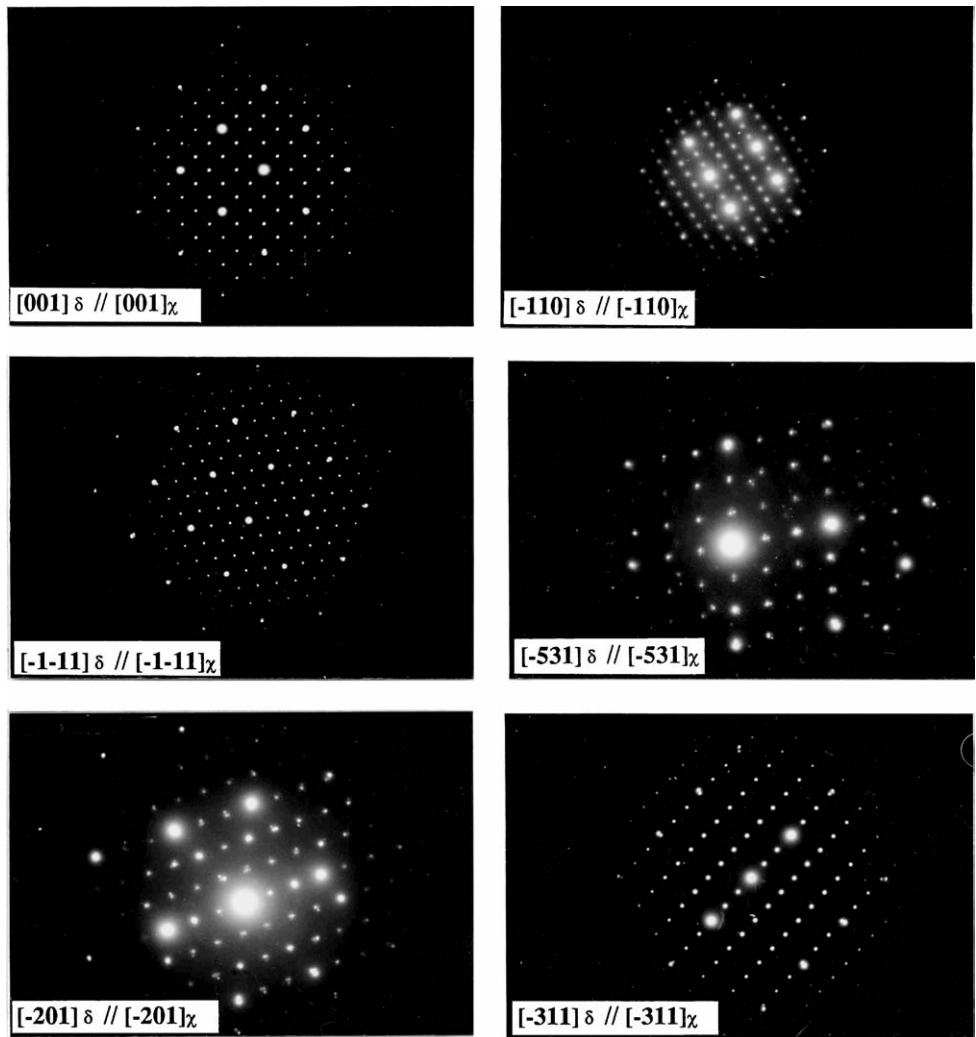
The χ -phase particles present at the δ/γ interfaces exhibit a rational orientation relationship with the austenite (Fig. 3b) with which it is in contact and the invariable cube-on-cube orientation relationship with the ferritic matrix into which it exclusively grows. It is relevant to point out that although the χ -phase adopts a cube-on-cube orientation relationship with the ferritic matrix, it does not inherit the well-known Kurdjumov-Sachs (K-S) orientation relationship usually observed between ferrite and austenite. The χ -phase develops the so-called Nishiyama-Wassermann (N-W) orientation relationship:

$$\begin{aligned} (1\ 1\ 0)_\chi & // (1\ 1\ 1)_\gamma \\ [1\ 1\ 0]_\chi & // [\bar{2}\ 1\ 1]_\gamma \\ [0\ 0\ 1]_\chi & // [0\ \bar{1}\ 1]_\gamma \end{aligned}$$

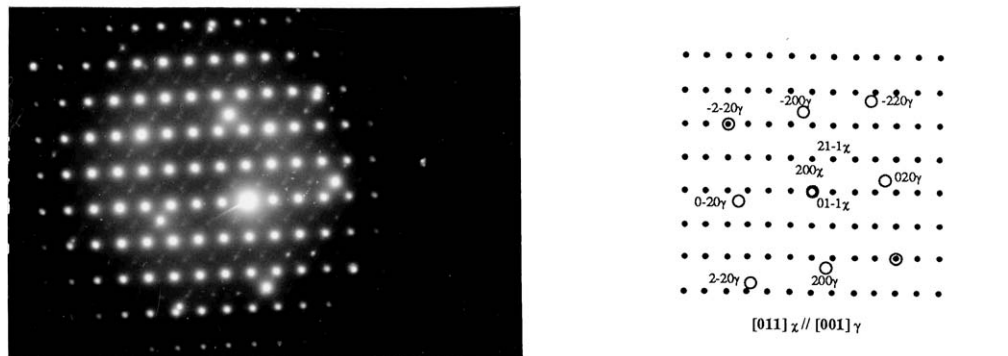
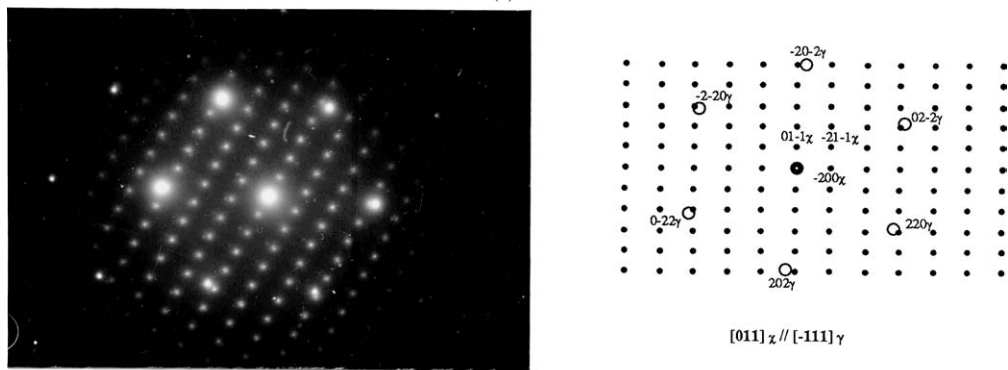
This orientation relationship is different from the one reported by Duhaj *et al.* [44] between the χ -phase and the austenitic matrix of a fully austenitic stainless steel. Finally, the following triangular orientation relationship (TOR):

$$(1\ 1\ 0)_\chi // (1\ 1\ 0)_\delta // (1\ 1\ 1)_\gamma$$

is observed between the χ -phase, the austenite and the ferritic matrix.



(a)



(b)

Figure 3 (a) Series of composite electron diffraction patterns recorded along different zone axes common to χ -phase particles and the surrounding δ -ferritic matrix. These diffraction patterns exhibit a cube-cube orientation relationship between the χ -phase and the δ -ferritic matrix. (b) Series of composite electron diffraction patterns recorded along zone axes common to χ -phase particles and the austenite and their indexations.

3.3.3. χ/σ orientation relationship

A preferential orientation relationship is also observed between the χ -phase and the intermetallic σ -phase and can be expressed as:

$$(1\ 1\ 0)_\chi // (0\ 0\ 1)_\sigma$$

$$[\bar{1}\ 1\ 1]_\chi // [1\ 1\ 0]_\sigma$$

$$[1\ \bar{1}\ 2]_\chi // [\bar{1}\ 1\ 0]_\sigma$$

In Section 4.3, it will be shown that the parallelism of planes of χ -phase, the austenite and the ferritic matrix can be interpreted by a common geometric approach.

The orientation relationship between the χ -phase and the austenite on the one hand and the χ -phase and σ -phase on the other hand are energetically favourable because they are characterized by a low misfit. This low linear dilatation explains, among other parameters, the favoured inter and intragranular nucleation followed by the transition from the δ -ferrite to the χ -phase.

In seeking to understand why the χ -phase, precipitated at the δ/γ interfaces does not inherit the K-S

orientation relationship usually observed between the ferrite and the austenite, will be considered in the following sections.

3.4. The χ/δ , χ/γ , χ/σ and γ/δ interfaces

As interfaces play a crucial role in the control of mechanical properties of alloys, they usually justify detailed investigation [45, 46]. In particular, the equilibrium of homophase as well as heterophase interfaces is assumed to be linked to the presence of intrinsic defects such as dislocations and/or ledges [47]. The χ/δ , χ/γ , χ/σ and γ/δ interfaces will be here analysed in terms of the orientation relationships between the phases situated on both sides of the interfaces.

Fig. 4 displays a χ -phase particle embedded in the ferritic matrix showing an array of dislocations at the χ/δ interface. Careful analysis of the electron diffraction patterns obtained at the χ/δ interfaces (Fig. 3a) reveals a departure from the perfect coherence since common spots of the χ and δ phases are not exactly superimposed. According to the fact that the χ -phase adopts a cube-on-cube orientation relationship with a lattice

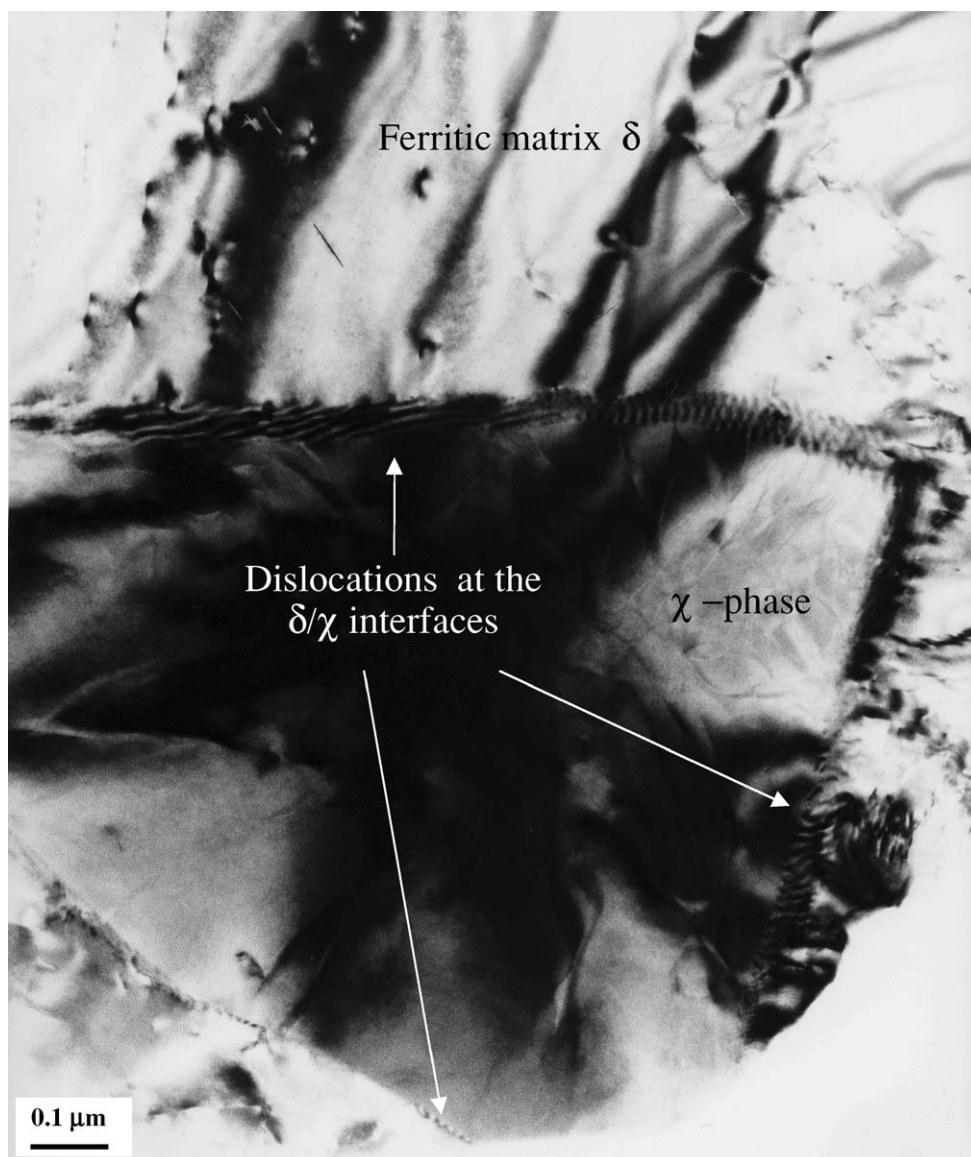


Figure 4 Array of dislocations at the interfaces between χ -phase particle and the surrounding ferritic δ -matrix.

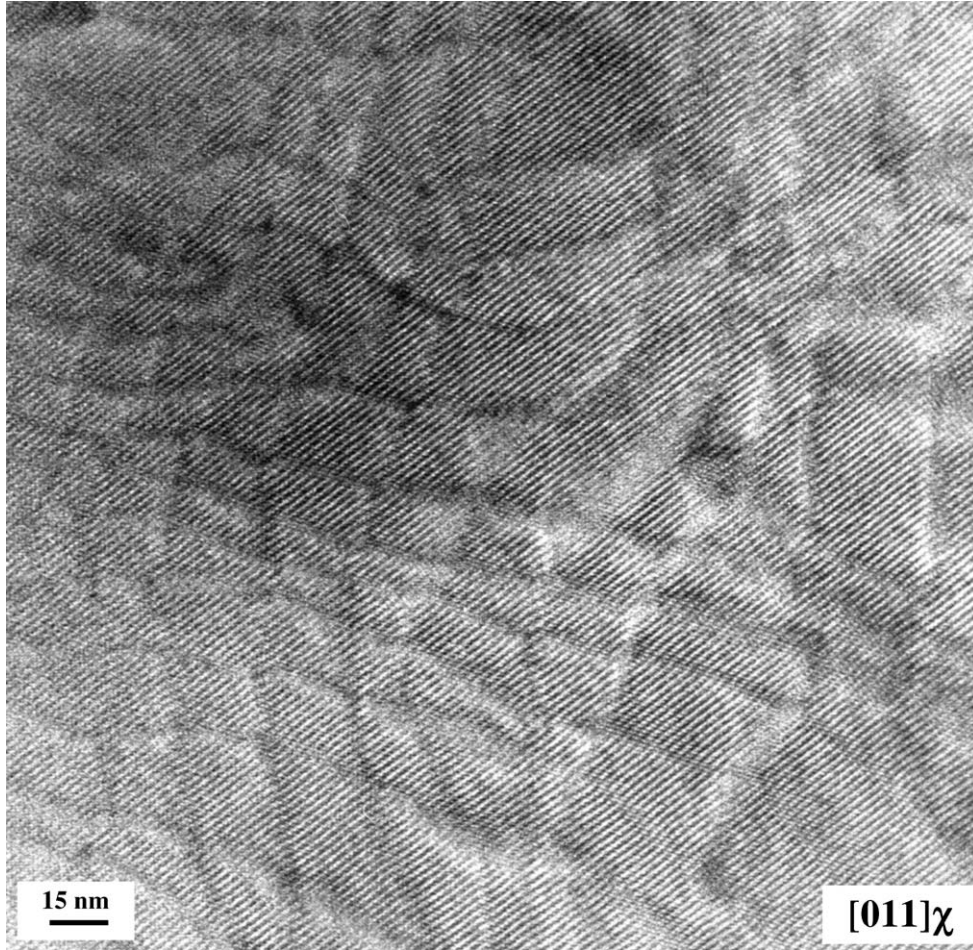


Figure 5 HREM image recorded along $[-110]$ zone axis showing that the χ -phase particles have a complex microstructure characterized by a network of boundaries separating very small domains.

parameter slightly larger than three times that of the ferritic matrix, the departure from coherence $\Delta_{[uvw]}$ along a $[uvw]$ direction can be expressed by:

$$\Delta_{[uvw]} = \frac{P_{[uvw]}^{\chi} - 3P_{[uvw]}^{\delta}}{P_{[uvw]}^{\chi}}$$

$P_{[uvw]}$ being the parameter of the $[uvw]$. For a cubic lattice, $P_{[uvw]} = a\sqrt{u^2 + v^2 + w^2}$.

The departure from coherence can be periodically and fully accommodated (without any long-range strain field) by the introduction of a dislocation net with a spacing D which span $3N$ atomic planes in the ferrite and $(N - 1)$ atomic planes in the χ -phase.

D and N are connected to $\Delta_{[uvw]}$ by:

$$D = \frac{P_{[uvw]}^{\chi}}{\Delta_{[uvw]}},$$

$$N = \frac{1}{\Delta_{[uvw]}}.$$

The interfaces between the χ -phase and the δ -matrix, determined by trace analysis (Fig. 1a), are parallel to the close-packed planes of the two structures, i.e., $(110)_{\chi} // (110)_{\delta}$. The main directions lying in these reference planes are $[001]$, $[-110]$, $[-111]$ and $[1-11]$. They exhibit a misfit $\Delta_{[uvw]} = 0.038$ (3.8%) and then

the deduced number of extra planes to be accommodated is $N = 26$.

3.5. Characterization of the defects

The uneven contrast pointed out by TEM observations (Fig. 1a, b and c) indicates that the χ -phase particles are characterised by a high density of defects. These defects are boundaries, which separate small domains whose size varies from 10 to 20 nm as illustrated by the HREM images (Fig. 5), though larger domains up to 70 nm can be also found. Examination of several Bright Field images such as Fig. 1c indicates that the χ particle defects are frequently roughly parallel to $\{110\}_{\chi}$ planes. The classical two beams extinction method has been used to determine the translation vectors associated with these boundaries. Five independent extinction conditions (Table IV) have been obtained. Solving the system of well-known equations $\mathbf{g} \cdot \mathbf{R} = \mathbf{n}$ has allowed determining their corresponding translation vectors as $1/4\langle 111 \rangle_{\chi}$ and $1/3\langle 110 \rangle_{\chi}$. Actually, these partial vectors are remarkably simple for structure as complex as the χ -phase one. Vector $R = 1/3\langle 110 \rangle_{\chi}$ corresponds to a simple translation between atomic sites in χ -cell that is not the case of $R = 1/4\langle 111 \rangle_{\chi}$. However it is worth noting that, because of the I-type Bravais χ -lattice, $R = 1/4\langle 111 \rangle_{\chi}$ fault vectors lead for any diffracting vector \mathbf{g} to a phase shift: $\phi = 2\pi \mathbf{g} \cdot \mathbf{R} = n\pi$. Hence these planar defects can be simply described as π boundaries.

TABLE IV Extinction conditions of χ -phase translation boundaries

Extinction conditions	Fault vector
$\bar{3}30$	$R = \frac{1}{4}[111]$
$\bar{1}4\bar{1}$	
$\bar{2}3\bar{3}$	
$\bar{2}3\bar{1}$	
$\bar{2}4\bar{2}$	$R = \frac{1}{3}[110]$
$\bar{3}30$	
$3\bar{3}2$	
$\bar{1}4\bar{1}$	
031	
444	

3.6. Chemical analysis

In an attempt to assess the composition of χ -phase, to establish the distribution of the alloying elements and to compare it to that of the ferritic matrix, microanalysis was performed using energy dispersive X-ray spectroscopy (EDS). Analyses were carried out in the thinnest areas of the sample, on particles very close to the electrochemical hole. Under these circumstances, the analysed area is fully located in the particle and the analysis is not biased by the matrix. The obtained results show that the chemical composition of the χ -phase is homogeneous from particle to particle. The chemical analysis results displayed in Table II indicate that the precipitation of χ -phase leads to an alteration of the surrounding ferritic-matrix.

4. Discussion

4.1. Misfit at the χ/δ interfaces

The geometrical analysis reported in Section 3.4 indicates that the χ/δ interfaces have a misfit corresponding to the introduction of one dislocation every 26 interplanar spacings. The interdislocation spacings would be 22.36 nm, 31.63 nm and 38.73 for $[001]$, $[-110]$ and $\{[-111]$ and $[1-11]\}$, respectively. In heterophase interfaces, rather than a misfit encountered along one direction, accommodation is better achieved along two directions by two sets of dislocations. The close-packed atomic directions (111) $\{[-111]$ and $[1-11]\}$ are the most favourable directions, for which the coherency strain fields can be decreased or completely relieved, leading then to a drop in the interfacial energy.

The dislocation arrays at the χ/δ interfaces (Fig. 4) reveal that the χ -phase particles can grow to a significant extent and remain semicoherent with the ferritic matrix. These arrays of dislocations are generated by the χ/δ misfit and/or by the thermal expansion misfit between the two phases. TEM observations leading to visibility of these interfacial dislocations under different reflections were consistent with having Burgers vectors of the type $\frac{1}{2}\langle 111 \rangle_\delta$. This result is in agreement with the considerations previously developed in Section 3.4.

Characterization of dislocations at the γ/χ and σ/χ heterophase interfaces, are not given here. However, analogy between χ/γ and δ/γ interfaces, suggest Burgers vectors of the $\frac{1}{2}\langle 110 \rangle_\gamma$ type at the χ/γ interface. In this field, HREM investigations are in progress to get more information about these interfaces and will be published elsewhere in more details.

4.2. The equilibrium shape of the intra and intergranular χ -phase particles

It is well established that the morphology of transformation products taking place in a solid matrix is of great importance in materials science. The equilibrium shape and the habit plane, respectively, adopted and developed between the transformation products and the parent phase have been extensively investigated. Both the morphology and the number of precipitate variants can be understood in terms of the group theory as developed elsewhere [48, 49]. This approach based on the shared symmetry elements of the two point groups of the product and parent phase could be applied to explain the χ -phase precipitation features. Let us consider the cube-on-cube orientation relationship developed by the χ -phase with the ferritic matrix, belonging to the point groups $G^\chi = 43m$ and $G^\delta = \frac{4}{m}\bar{3}\frac{2}{m}$, respectively. The intersection point group of G^χ and G^δ is represented by their common symmetry elements when the precipitate adopts an orientation relationship with the matrix [48, 49]. This intersection point group, labelled $H(G^\delta \cap G^\chi)$, is one of the 32 crystallographic point groups and a subgroup of the matrix and of the precipitate. For the cube-on-cube orientation relationship, the symmetry analysis becomes trivial (Table V): the mirrors, the inversion 4-fold and the 3-fold axes,

TABLE V Determination of the intersection point group H , the element of which are common to the χ and δ , χ and γ and χ and σ . n is the number of variants

	Orientation relationship	Superimposed symmetries	Shared symmetries	H	$n = \frac{m}{h}$
Cube-on-cube orientation relationship between χ and δ	$(001)_\chi // (001)_\delta$	4 on $4/m$	$\bar{4}$	$\bar{4}3m$	2
	$(011)_\chi // (011)_\delta$	m on $2/m$	m		
	$(111)_\chi // (111)_\delta$	3 on $\bar{3}$	3		
N-W orientation relationship between χ and γ	$(110)_\chi // (111)_\gamma$	m on 3	1	2	24
	$[\bar{1}10]_\chi // [\bar{2}11]_\gamma$	m on 1	1		
	$[011]_\chi // [0\bar{1}1]_\gamma$	$\bar{4}$ on $2/m$	2		
Orientation relationship between χ and σ	$(110)_\chi // (001)_\sigma$	m on $4/m$	m	m	24
	$[111]_\chi // [\bar{1}10]_\sigma$	3 on $2/m$	1		
	$[1\bar{1}2]_\chi // [110]_\sigma$	1 on $2/m$	1		

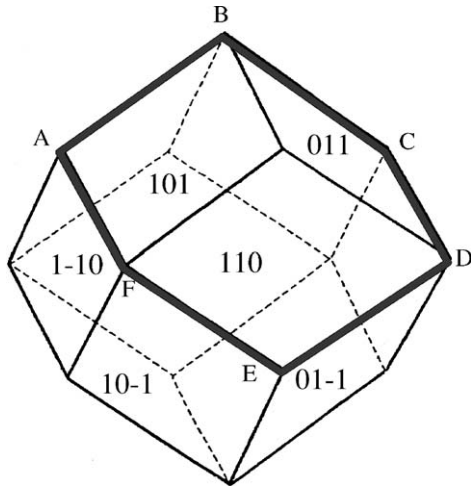


Figure 6 Rhombic dodecahedron the faces of which are $\{110\}$; the front faces are indexed. The projection of the rhombic dodecahedron leads to a hexagonal shape when viewed along $\langle 111 \rangle$ direction. The hexagonal shape (Fig. 1a) is parallel to an equatorial section (ABCDEF) of the rhombic dodecahedron when viewed along $\langle 111 \rangle$ direction. The hexagonal shape (Fig. 1a) is in fact compound of the projection along $\langle 111 \rangle$ of three $\{110\}$ faces related by one 3-fold axis of symmetry, i.e., $\langle 111 \rangle$ axis.

common to the point groups of the ferritic matrix and the χ -phase survive to the intersection point group. The resulting common point group is:

$$H = (G^\delta \cap G^\chi) = \frac{4}{m} \bar{3} \frac{2}{m} \cap \bar{4}3m = \bar{4}3m$$

This cubic point group, the order of which is 24 [50], dictates the shape of χ -phase particles. Under these circumstances, the χ -phase will develop a shape as it does in an isotropic medium [49]. For this point group, the developed general form consists of twenty-four faces, hexatetrahedra [51, 52]. The special forms are $\{111\}$ and $\{1\bar{1}1\}$, tetrahedra; $\{100\}$, a cube; and $\{110\}$, which consists of twelve faces [51, 52]. In this study, the special form developed by the χ -phase is a rhombic dodecahedron (Fig. 6) the faces of which are $\{110\}$ [51, 52]. Every face is a parallelogram delimited by $\langle 111 \rangle$ edges. The special equilibrium shape is consistent with the one experimentally observed. The $\{110\}$ faces of the χ -phase have been determined by trace analysis involving several orientations of the δ matrix grains. Observation of hexagonal plates (Fig. 1a) is indeed consistent with a rhombic dodecahedron particle projected along a $\langle 111 \rangle$ direction. The experimentally observed hexagonal shape is in fact compound of the projection of three $\{110\}$ faces, which are related by one 3-fold axis (Fig. 1a). One can note on passing that $\bar{4}3m$ corresponds to a symmetry dictated extremum with respect to arbitrary rotation [48, 49]. However, the number (n) of variants defined as the ratio of the order of G^δ (m) to that of $H(h)$, is equal to 2 [50]. This means that for the χ -phase, there are 2 variants that could take place in every grain of the ferritic matrix.

The shape of the χ -phase particles developed at the γ/δ interface and expanding in the ferritic matrix, can also be understood in term of the shared symmetry elements between the austenite and the χ -phase. For

the N-W orientation relationship exhibited between the austenite and the χ -phase, the derived intersection point group (Table V) is:

$$H = (G^\gamma \cap G^\chi) = \frac{4}{m} \bar{3} \frac{2}{m} \cap \bar{4}3m = 2$$

This intersection point group is monoclinic of order 2. Twenty four possible variants of χ -phase particles would, therefore be expected. The special shape belonging to this $H = 2$ are pedions or pinacoids. The latter shape are consistent with the one experimentally observed (Fig. 1b). In this case, the observed morphology corresponds to the symmetry dictated extremum which is obtained when $(\frac{2}{m})_\gamma$ is parallel to $(\bar{4})_\gamma$ (49).

The shape adopted by χ -phase particle developed at the σ/δ interface and expanding in the ferritic matrix can also be explained in term of the shared symmetry elements. The point group of the σ -phase is $G^\sigma = \frac{4}{m} \frac{2}{m} \frac{2}{m}$. Taking into account the orientation relationship, which relates the two phases, the intersection point group, H , which dictates the shape of the χ -phase particle (Table V) is:

$$H = (G^\sigma \cap G^\chi) = \frac{4}{m} \frac{2}{m} \frac{2}{m} \cap \bar{4}3m = m$$

The latter is monoclinic of order 2 characterised by pedions or pinacoids. The experimentally observed particle seem to have an unspecified shape (Fig. 1c). The departure to the dictated shape is related to the fact that the analysed particles are not observed at the early stage of their formation. Actually a pinacoid morphology is not very specific, it is then possible that particle showing a planar interface parallel to $(001)_\sigma$ (Fig. 1c) may have a pinacoid shape, i.e., a pair of parallel faces, in a coarsening stage.

4.3. Geometrical and chemical considerations

Despite the complexity of the χ -phase, the study of microstructure defects, orientation relationship as well as interface planes reveal several simple geometric relations between the χ -phase and the ferritic matrix. This has suggested us to adopt a geometrical point of view in order to examine the relation between the χ -phase and the ferrite. In a second step, the meaning of the geometrical similarities, using the chemical information gained from EDS analysis, will be discussed.

4.3.1. Geometrical analysis

The unit cell of χ -phase as all the isostructures of α -Mn contains 58 atoms, which occupy, from the "International Tables for Crystallography" [42], the positions reported in Table I. Since the cell parameter of the χ -phase is approximately 3 times that of the ferrite and taking into account the cube-on-cube orientation relationship, the χ -phase cell can be expressed as a super-cell containing 27 ferrite unit cells. Such superstructure would contain 54 atoms (2×27); the

BCC ferritic matrix has 2 atoms per unit cell. However, the χ -phase cell is known to hold 58 atoms. Using the exact cell parameter of the χ -phase and of the ferrite, we obtained for the respective atomic density ρ 0.0122 nm³/atom for the χ -phase and 0.0118 nm³/atom for the ferrite, that corresponds to an enhancement of 3.3%.

Considering the δ/χ , the γ/χ and σ/χ interfaces as well as the π boundaries in the χ -phase, it is worth noting that all these microstructures involve the (110) χ -phase plane. This plane seems then to play a key role in the χ -structure. A projection of the atoms of the cell of χ -phase along $\langle 001 \rangle$ direction (Fig. 7a), represented using commercial software (CaRine[®] Boudias and Diligent), shows that it can be described as a stacking of atomic planes (A to G) (Fig. 7a), which are nearly equidistant and parallel to (110) plane. Although most of the atoms of the six layers are on a plane of the cell, others are aside from it. In these latter cases the calcu-

lated separations are much shorter than an interatomic distances. Under these circumstances, the atomic distribution of the χ -phase should be described as a stacking of corrugated layers parallel to the (110) planes (Fig. 7b). Three sets of layers may be distinguished in (Fig. 7a). The set, including A, D and G layers, is the least compact of the three types (Fig. 7c). The second one, represented by B and E layers (Fig. 7c), is the more compact, and the last set, which includes C and F layers (Fig. 7c) shows an intermediate compactness between the former two.

It is remarkable that B and E set has the same density as that of $\{110\}$ planes in ferrite. Then, the δ/χ interface implying the dense $\{110\}$ ferrite planes parallel to the corrugated set of layers B and E, realizes the conservation of atomic sites density. Such an approach, developed elsewhere [53], has already allowed the interpretation of interface observed between the χ and σ Frank-Kasper phases. In that work, the point was to

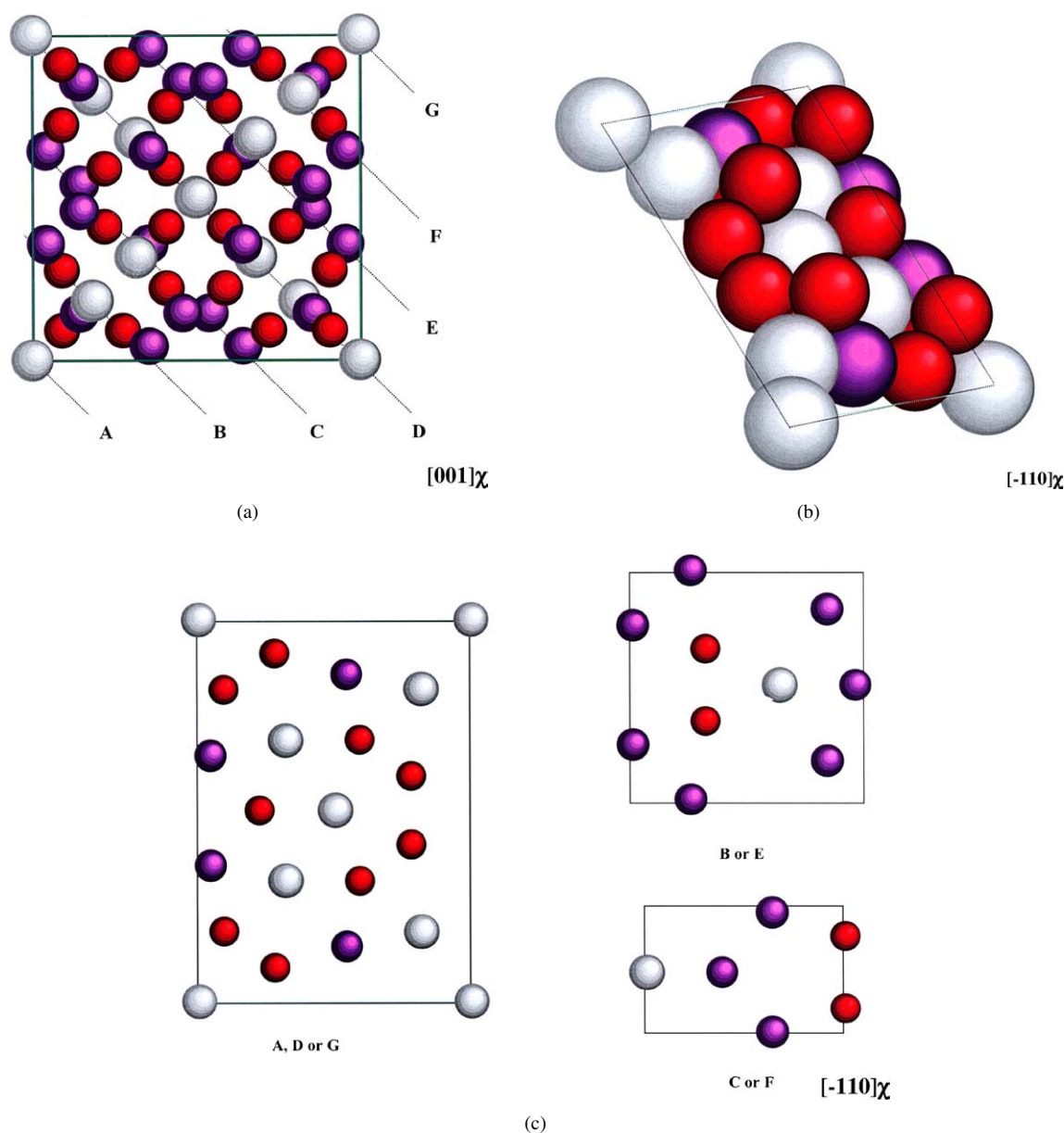


Figure 7 (a) Projection of the atoms of the χ -phase cell along $[001]$ direction. The atoms are situated on planar and corrugated layers (A to G) compiled parallel to (110) plane. (b) Atoms belonging to the layers A (D or G). (c) Projection of the atoms on layers (A, D or G), (B or E) and (C or F).

explain the selection of some planes as interfaces by the possibilities of having a bounded transformation that is a local rearrangement at the interface plane. Considering thick layers in the Frank-Kasper σ -phase, in an analogous manner as the sets of layers described here, it was observed that atomic sites density was conserved through the interface plane. Both approaches have pointed out the particular part played by the $(110)_\chi$ corrugated layer. Actually, the density explains why this corrugated layer has a specific meaning: it is equivalent to a compact plane. The two (110) -corrugated layers are related by a vector of $1/4\langle 111 \rangle_\chi$ type. This geometrical observation provides a natural interpretation for π boundaries observed in the χ -phase. The conservation of density at the interfaces between $(001)_\sigma$ and $(110)_\chi$ thick layers on one hand and between $\{110\}$ ferrite dense planes and $(110)_\chi$ thick layers on the other hand, implies that atomic density is conserved between (001) thick layers of the σ -phase and the dense $\{110\}$ ferritic plane at the σ/δ interface. Actually, all the different interfaces observed in the duplex stainless steels, interfaces mentioned above as well as the austenitic-ferritic K-S interface, involve dense planes or dense corrugated layers and correspond to the conservation of atomic density at the interface.

Such geometrical analysis of defects might be of interest in connection with mechanical properties since Zakine [54] has evidenced by tensile tests, that these planar defects are responsible for the brittleness of the χ -phase particles. However, this geometrical approach has completely neglected the chemical aspects, which need actually to be analysed in order to understand the meaning of the noticed geometrical properties.

4.3.2. Chemical point of view

Compared to the chemical composition obtained from the adjacent δ -ferrite, the χ -phase particles are evidently enriched in Mo and depleted in Fe: 20 times and 3/4 times as much as in the matrix, respectively. However, it is interesting to note that the sums of both concentrations (Fe + Mo) are the same in the two phases, but Mo largely substitutes Fe in the χ -phase. This feature seems to support conclusively the idea that Mo promotes the precipitation of the χ -phase as it does for the other τ and R intermetallic phases [18, 19]. Microanalysis undertaken across the particles of χ -phase formed between 650 and 750°C indicates that the temperature has no effect on the chemical composition [13].

The fact that the χ -phase takes place in the matrix later in time than the σ -phase is consistent with the assumption that the incubation time for χ -phase formation is associated with the diffusivities of its stabilizers elements (Mo, . . .) in the ferritic matrix. Indeed, the diffusion rate of Mo is lower than that of the other transition metals in the ferrite.

The analysis of the similarities between the distribution of the atoms in the χ -phase and in the ferritic super-cell now allows us to say that the alteration of the ferritic matrix during the formation of the others phases: austenite and σ -phase leads to an unstable ferrite. When the ferritic matrix reaches a critical chem-

ical composition close to that of the χ -phase, the latter precipitate under favourable conditions by atomic position readjustments whose amplitudes are smaller than the interatomic distances. This situation is clearly pointed out by the schematic projection (Fig. 8a) of the atoms of the two phases onto the $(110)_\delta // (110)_\chi$ plane. The incubation time recorded for the χ -phase formation corresponds to the length of time to reach a critical composition

It has been pointed out that the χ -phase is related to the austenite by the N-W orientation and does not inherit the K-S orientation between the austenite and the ferrite. The χ -phase is strongly affected by the crystallographic orientation relationship at δ/γ interface. In order to understand this situation, let us recall that the two orientations K-S and N-W are theoretically related by a low rotation of 5.26° along the common $\langle 110 \rangle_\delta // \langle 111 \rangle_\gamma$ direction. Penisson *et al.* [55] have brought to light that the orientation between the ferritic matrix and the austenite precipitating at high temperature is not constant and is varying in the angular domain contained between K-S and N-W relationships. This deviation is related to the variation of the a_γ/a_δ parameters ratio and are localised, as established by Dahmen [56], between the exact N-W and K-S orientations. It has also been observed that the orientation between the two structures is related to different parameters, among them alloy purity [57, 58] and heat treatments [58]. These parameters can modify the interface (boundary) structure by locally accommodating the structure and thus favouring one orientation to the detriment of the other. The projections of $(111)_\gamma$ plane onto the $(110)_\chi$ plane according to K-S or N-W are very close and the passage from the former to the latter can occur easily. This situation is illustrated by the schematic representation of the two orientations (Fig. 8b and c) and clearly confirms the fact that N-W corresponds to a partial extremum dictated by the symmetry [48, 49]. As suggested by Cahn and Kalonji [49], this extremum should not be a deep one, making possible the passage from the K-S to N-W.

5. Summary and conclusions

The isothermal heat treatment of duplex stainless steel in the temperature range between 600 and 970°C leads to a series of phase transformations which take mainly place in the ferritic matrix and at its interphase boundaries. This investigation has been concentrated on the χ -phase, an intermetallic compound rich in Cr and Mo, precipitated within the ferritic matrix. These particles are examined using a combination of several TEM techniques, crystallographic as well as analytical. Besides, in the electron diffraction and morphology study, we particularly emphasize on the symmetry analysis.

This χ -phase nucleates also at the δ/γ and δ/σ interfaces and grows by expanding exclusively in the ferritic matrix enriched in intermetallic forming (Cr, Mo.) elements during the $\delta \rightarrow \gamma$ transformation of a Fe-22Cr-5Ni-3Mo-0.03C duplex stainless steel. The χ -phase appears, with an incubation time, after the formation of the austenite and the intermetallic σ -phase. The

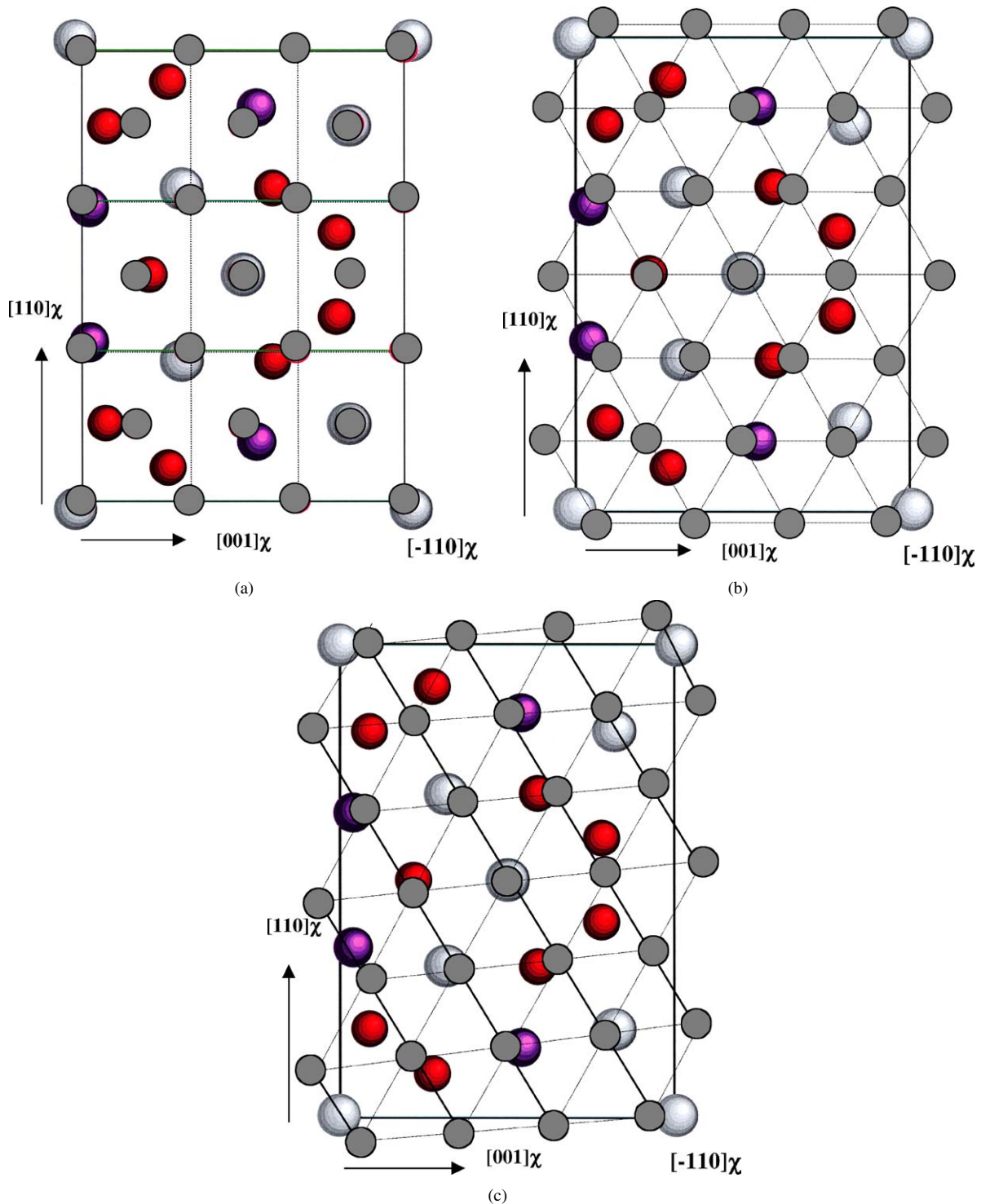
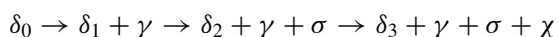


Figure 8 (a) Superimposition of the layer A (D or G) on the (110) δ -ferritic plane according to the cube-on-cube orientation relationship. The projection shows the atomic displacements for $\delta \rightarrow \chi$ transition. (b) Superimposition of the layer A (D or G) on the (111) austenitic plane according to the Nishiyama-Wasserman orientation relationship. The projection shows the atomic displacements for $\gamma \rightarrow \chi$ transition. (c) Superimposition of the layer A (D or G) on the (111) austenitic plane according to the Kurdjumov-Sachs orientation relationship. The projection shows the atomic displacements for $\gamma \rightarrow \chi$ transition.

precipitation sequence the alloy undergoes can be written as follows:



The δ_0 phase is the primeval supersaturated and fully ferritic matrix. The phases δ_1 , δ_2 and δ_3 correspond to ferritic matrices whose chemical composition are in equilibrium with γ , $\gamma + \sigma$ and $\gamma + \sigma + \chi$, respectively. The austenite and the intermetallic σ -phase obviously

have low activation energy barrier for nucleation than the χ -phase.

The characterization by electron microdiffraction determines unambiguously that the χ -phase crystallizes in the cubic system and belongs to $I\bar{4}3m$ space group. The results of this electron diffraction characterization are in agreement with those reported from X-ray and neutron diffraction experiments. The electron diffraction patterns analyses point out that the χ -phase adopts an orientation relationship with the

ferritic matrix in which it develops and rational orientation relationships with the austenite and the σ -phase with which it is in contact. These orientation relationships are: cube-one-cube: $(hkl)_\chi // (hkl)_\delta$ with the ferrite, Nishiyama-Wasserman type: $(110)_\chi // (111)_\gamma$; $[001]_\chi // [0\bar{1}1]_\gamma$ with the austenite and finally $(110)_\chi // (001)_\sigma$; $[\bar{1}11]_\chi // [110]_\sigma$ with the σ -phase. The fact that these orientations are obeyed is connected to the occurrence of good matching between the $(110)_\chi$ reference plane and the corresponding planes belonging to the other γ and σ phases. These rational orientation relationships ensure structural continuity between the ferritic matrix and the intergranular χ -phase on one hand, and with the intergranular χ -phase via the heterophase δ/γ and δ/σ interfaces, on the other hand.

The χ -phase particles developed at the heterophase interfaces adopt a pinacoid like morphology while those formed inside the ferritic grains exhibit a rhombic dodecahedron form. These shapes and the variant numbers developed inside of the ferritic grains and at the heterophase interfaces are understood in term of the group theory.

TEM observations and electron diffraction analyses revealed that χ -phase particles are heavily faulted. The defects identified as π boundaries obey roughly the following parallelism $\{011\}_\chi // \{011\}_\delta$. The associated fault vectors are identified as: $1/3\langle 110 \rangle_\chi$ and $1/4\langle 111 \rangle_\chi$ types.

Based on its crystallographic data and the orientation relationship that it develops with the ferritic matrix, the χ -phase can be considered as a ferritic super-cell with the same atomic density. Similarly, the χ -phase can be described as a set of corrugated and planar layers related to each other by simple partial vectors and obeying the following parallelism $\{011\}_\chi // \{011\}_\delta$.

Because of the persistence of simple geometrical features (interface, fault planes and fault vectors), the complex χ -phase structure has been considered under a simple geometrical point of view focused on the atomic density regardless of the composition. In this approach, interfaces as well as fault planes obey to a conservation rule of site density.

According to the local chemical analysis, there is a substitution of Fe atoms by Mo atoms. The geometrical analysis suggests that the diffusion is a short range one and is associated to small displacement. Finally the χ -phase, in spite of its complexity remains in close geometrical relation with the ferritic matrix.

Actually the possibility of complex organisation of χ -phase is certainly one of the more puzzling features of the χ -phase which has not been developed in this paper which rather focuses on aspect of metallurgic interest. In the χ -phase particles, the density of defects may become extremely high which indicate low fault energy as well ability of the χ -phase to tolerate heavy distortion. In the very highly faulted χ -phase particles, structural anomalies have been noticed. These anomalies are characterised by aperiodic electron diffraction patterns [59]. Similar aperiodic diffraction patterns have been also observed in Fe-Cr-Mo, V-Ni-Si, V-Ni-Co, Mg-Al alloys obtained by rapid solidification. The common point of

these systems and the χ -phase is to be isostructural of the α -Mn structure. This is indeed another reason for considering the Frank-Kasper type phases according to a geometrical point of view, since the topology of the packing seems to be responsible for common structural properties, the sensitivity to chemical composition being then a second order phenomenon.

References

1. R. M. DAVISON and J. M. REDMOND, *Mater. Perform.* **29** (1990) 57.
2. H. KIESHEYER, in Proceedings of the International Conference on Stainless Steels' 91 (The Iron and Steel Institute of Japan, Chiba, Japan 1991) p. 1148.
3. V. J. DIGGS, W. D. BUSKO and C. M. SCHILLMOLLER, in Proceedings of the International Conference on Duplex Stainless Steels'91, edited by J. Charles and S. Bernhardsson (Les Editions de Physique, Les Ulis, 1991) Vol. 2, p. 1163.
4. D. J. A. FRUYTIER, in Proceedings of the International Conference on Duplex Stainless Steels'91, edited by J. Charles and S. Bernhardsson (Les Editions de Physique, Les Ulis, 1991) Vol. 1, p. 497.
5. I. TAMURA and Y. TOMOTA, in Proceedings of the Symposium on Mechanical Behaviour of Materials (Japan Society of Materials Science, Kyoto, 1974) Vol. 2, p. 105.
6. J. FOCT, N. AKDUT and G. GOTTSTEIN, *Scripta Metall. Mater.* **27** (1992) 1033.
7. N. SRIDHAR, J. KOLTS and L. H. FLASCHE, *J. Metals* **37** (1985) 31.
8. T. MAGNIN and J. M. LARDON, *Mater. Sci. Eng. A* **104** (1988) 21.
9. S. BERNHARDSSON, J. OREDSSON and C. MARTENSON, in Proceedings of the International Conference on Duplex Stainless Steels'82, edited by R.A. Lula (ASM, Metals Park, Ohio, 1983) p. 267.
10. J. C. PROUHEZE, J. C. VAILLANT, G. GUNTZ and B. LEFEBVRE, in Proceedings of the International Conference on Duplex Stainless Steels'82, edited by R.A. Lula (ASM, Metals Park, Ohio, 1983) p. 247.
11. H. D. SOLOMON, in Proceedings of the International Conference on Duplex Stainless Steels'82, edited by R. A. Lula (ASM, Metals Park, Ohio, 1983) p. 41.
12. J. CHARLES, in Proceedings of the International Conference on Duplex Stainless Steels'91, edited by J. Charles and S. Bernhardsson (Les Editions de Physique, Les Ulis, 1991) Vol. 1, p. 3.
13. A. REDJAÏMIA, Thèse de Doctorat d'Etat, Institut National Polytechnique de Lorraine (Nancy, France, 1991).
14. A. REDJAÏMIA and G. METAUER, *J. Mater. Sci.* **36** (2001) 1717.
15. A. REDJAÏMIA, G. METAUER and M. GANTOIS, *Scripta Metall. Mater.* **25** (1991) 1879.
16. R. LAGNEBORG, *Trans. Amer. Soc. Metals* **60** (1967) 67.
17. A. MATEO, L. LLANES, M. ANGLADA, A. REDJAÏMIA and G. METAUER, *J. Mater. Sci.* **32** (1997) 4533.
18. A. REDJAÏMIA, P. RUTERANA, G. METAUER and M. GANTOIS, *Phil. Mag. A* **67**(5) (1993) 1277.
19. A. REDJAÏMIA, J. P. MORNIROLI, P. DONNADIEU and G. METAUER, *J. Mater. Sci.* **37** (2002) 4079.
20. E. L. BROWN and G. GRAUSS, *Metall. Trans.* **14** (1983) 791.
21. K. W. ANDREWS and P. E. BROOKES, *Metal Treatm. Drop Forg.* (1951) 301.
22. J. G. MCMULLIN, S. F. REITER and D. G. EBELING, *Trans. ASM* **46** (1954).
23. J. S. KASPER, *Acta Metall.* **2** (1954) 456.
24. A. J. BRADLEY and J. THEWLIS, *Proc. Roy. Soc. A* **115** (1927) 456.
25. F. C. FRANK and J. S. KASPER, *Acta Cryst.* **11** (1958) 305.
26. TAE-HOE LEE and SUNG-JOON KIM, *Scripta Materialia* **39**(7) (1998) 951.

27. I. C. I. OKAFOR and O. N. CARLSON, *Metall. Trans. A* **9A** (1978) 1651.
28. A. M. RITTER, J. MICHAEL, J. CIESLAK and W. F. SAVAGE, *Metall. Trans. A* **14** (1983) 37.
29. J. GOLDSMITH, "Interstitial Alloys" (Plenum Press, New York, 1967) p. 167.
30. B. WEISS and R. STICKLER, *Metall. Trans.* **3** (1972) 851.
31. J. E. SPRUIELL, J. A. SCOTT, C. S. ARY and R. L. HARDIN, *ibid.* **4** (1973) 1533.
32. YONG JUN OH and JUN HWA HONG, *J. Nucl. Mater.* **278** (2000) 242.
33. J. LAI, *Mater. Sci. Eng.* **58** (1983) 195.
34. J. K. LAI and J. R. HAIGH, *Weld J.* **58** (1979) 1s.
35. J. O. NILSSON, A. WILSON, B. JOSEFSSON and T. THORVALDSSON, in Proc. Stainless Steels '92 (Institute of Metals, 1992) Vol. 1, p. 280.
36. P. SHANKAR, H. SHAIKH, S. SIVAKUMAR, S. VENUGOPAL, D. SUNDARARAMAN and H. S. KHATAK, *J. Nucl. Mater.* **264** (1999) 22.
37. P. DUHAJ, J. IVAN and E. MAKOVICKY, *J. I. S. I.* **206** (1968) 1245.
38. F. A. THOMPSON and D. R. F. WEST, *ibid.* (1972) 691.
39. B. WEISS and R. STICKLER, *Metall. Trans.* **3** (1972) 851.
40. B. F. BUXTON, J. A. EADES, J. W. STEEDS and G. M. RACKHAM, *Philos. Trans. R. Soc.* **281** (1976) 171.
41. J. P. MORNIROLI and J. W. STEEDS, *Ultramicroscopy* **45** (1992) 219.
42. "International Tables for Crystallography", edited by T. HAHN (Reidel, Dordrecht, 1988).
43. C. ZAKINE, J. L. BECHADE and C. PRIOUL, *Scripta Mater.* **34**(9) (1996) 1399.
44. P. DUHAJ and J. IVAN, *J. I. S. I.* **206** (1968) 1014.
45. A. W. BOLLMANN, *Phys. Stat. Sol. (a)* **21** (1974) 543.
46. B. R. W. BALLUFI, A. BROKMANN and H. KING, *Acta Metall.* **30** (1982) 1453.
47. C. J. H. VANDER MERWE, in Proceedings of the Royal Society (London, 1949) Vol. 198, p. 205.
48. R. PORTIER and D. GRATIAS, *J. Phys. Sup.* **43**(12) (1982) C4-17.
49. J. W. CAHN and G. KALONJI, in Proceedings of the Conference on Solid-Solid Phase Transformations, edited by H. I. Aaronson, R. F. Seeker, D. E. Laughlin and C. M. Waymann (Metal. Soc. AIME, Warrendale, 1982) p. 3.
50. M. J. BUERGER, "Elementary Crystallography" (Massachusetts Institute of Technology Press, Cambridge, 1978).
51. F. C. PHILLIPS, "An Introduction to Crystallography," 4th ed. (Longman, Singapore, 1971).
52. D. MCKIE and C. MCKIE, "Essentials of Crystallography" (Blackwell Scientific Publications, Oxford, 1986).
53. A. PROULT and P. DONNADIEU, *Phil. Mag. Let.* **5**(72) (1995) 337.
54. C. ZAKINE, PhD thesis, Ecole Centrale de Paris, France, 1994.
55. J. M. PENISSON and G. REGHEERE, *Mater. Sci. Eng.* (1989) 199.
56. U. DAHMEN, *Acta Metall.* **30** (1982) 63.
57. M. EL HAJJAJI, Thèse de Doctorat d'Etat, Université Claude Bernard-Lyon, 1986.
58. C. P. LUO, U. DAHMEN, M. J. WITCOMB and K. H. WESTMACOTT, *Scripta Metall. Mater.* **26** (1992) 649.
59. P. DONNADIEU and A. REDJAIMIA, *J. Phys. I France* **5** (1995) 1.

*Received 14 May
and accepted 13 November 2003*